4

Enhancement of Wind Energy Penetration Levels using Adaptive LMF Control Algorithm

This chapter presents the Least Mean Fourth controlled DSTATCOM based method for enhancing wind energy penetration level in the rural grid by mitigating the PQ disturbances under the MATLAB and experimental environments. Power quality issues associated with variable wind speeds, different grid strength, loads composition, and wind penetration levels have been investigated. Finally, the effectiveness of the proposed algorithm has been compared using algorithms published in the literature.

4.1 INTRODUCTION

In the rural grids, the large scale Wind Energy (WE) penetration tends to increase largely because of unlimited availability and reduced carbon emissions [Aguero *et al.*, 2019]. These grids require smart features like small installation and running costs, less maintenance during operation, low power loss, and high-quality power to meet the load demand. Doubly Fed Induction Generator (DFIG) based WE sources are vital to those solutions, as they can provide continuous electric power day and night without any specific energy storage device. However, the high capacity of DFIG based WE connected to the weak end of the grid has presented multiple challenges to utilities due to the inconsistent wind output, connected loads, interfacing converters, and strength of the AC grid. [Chi *et al.*, 2019], established that the accurate reactive power planning and additional DSTATCOM structure can resolve the said challenges and enable a high WE penetration level. Therefore, an appropriate control algorithm for DSTATCOM is required to adapt to the changes associated with the changes in the system and generate optimum switching signals.

4.2 MERITS OF ADAPTIVE LMF CONTROL ALGORITHM

The proposed work aims to enhance WE penetration levels of the rural grid in the presence of NL loads. The additional DSTATCOM infrastructure is proposed in this thesis for improving the PQ and managing the reactive power requirement at PCC during high WE penetration. The adaptive LMF algorithm is implemented for the control of DSTATCOM. The proposed algorithm works on continuous updating of weight components of current and voltage signals based on changes in the system for the estimation of reference gate signals. The performance of the proposed adaptive control algorithm is improved by considering more operating points.

The phase-locked loop (PLL) based schemes are applied for obtaining the phase and frequency of the voltage at the PCC [Muyeen, 2014; Givaki *et al.*, 2019; Hu *et al.*, 2015]. These methods work well under stiff grid and linear load conditions. However, in the case of the weak grid and NL loads, the PLL has a negative resistance, which causes instability, PQ issues and limits the power transfer of WE sources in low SCR grids. Suppression Technique (ST) performance was unsatisfactory for the SCR of less than 4 in [Peng *et al.*, 2021]. However, the research studies in [Mosaad, 2018; Chi *et al.*, 2019; Li *et al.*, 2019a; Peng *et al.*, 2021; Li *et al.*, 2020a; Zhang *et al.*, 2020;

Jabbarnejad *et al.*, 2020; Chishti *et al.*, 2020; Restrepo and Rios, 2019] presented the capabilities of the adaptive control for mitigating instability and reactive power issues. Still, their performances did not examine under the conditions of different grid strengths, wind speeds and non-linear loads, which is essential for the rural grid application. The proposed adaptive control algorithm ensures reliable operation with maintaining PQ standards due to the attractive features, including simple architecture, self-adjustment function, simplified calculation, Experimental compatibility, PLL-less structure, adaptiveness, minor steady-state error, and accuracy of estimation of power.

4.3 SYSTEM CONFIGURATION

The system configuration of the weak rural grid with high WE penetration is depicted in Fig. 4.1, where the DSTATCOM is employed to inject the required reactive power and improve the PQ for enhancement of WE penetration into the rural grid. The base MVA and base voltage are selected to be 4.5 MW and 0.415 kV, respectively, for the per-unit (p.u.) calculations. The details of the various parameter used for the system configuration is presented in Table 4.1.

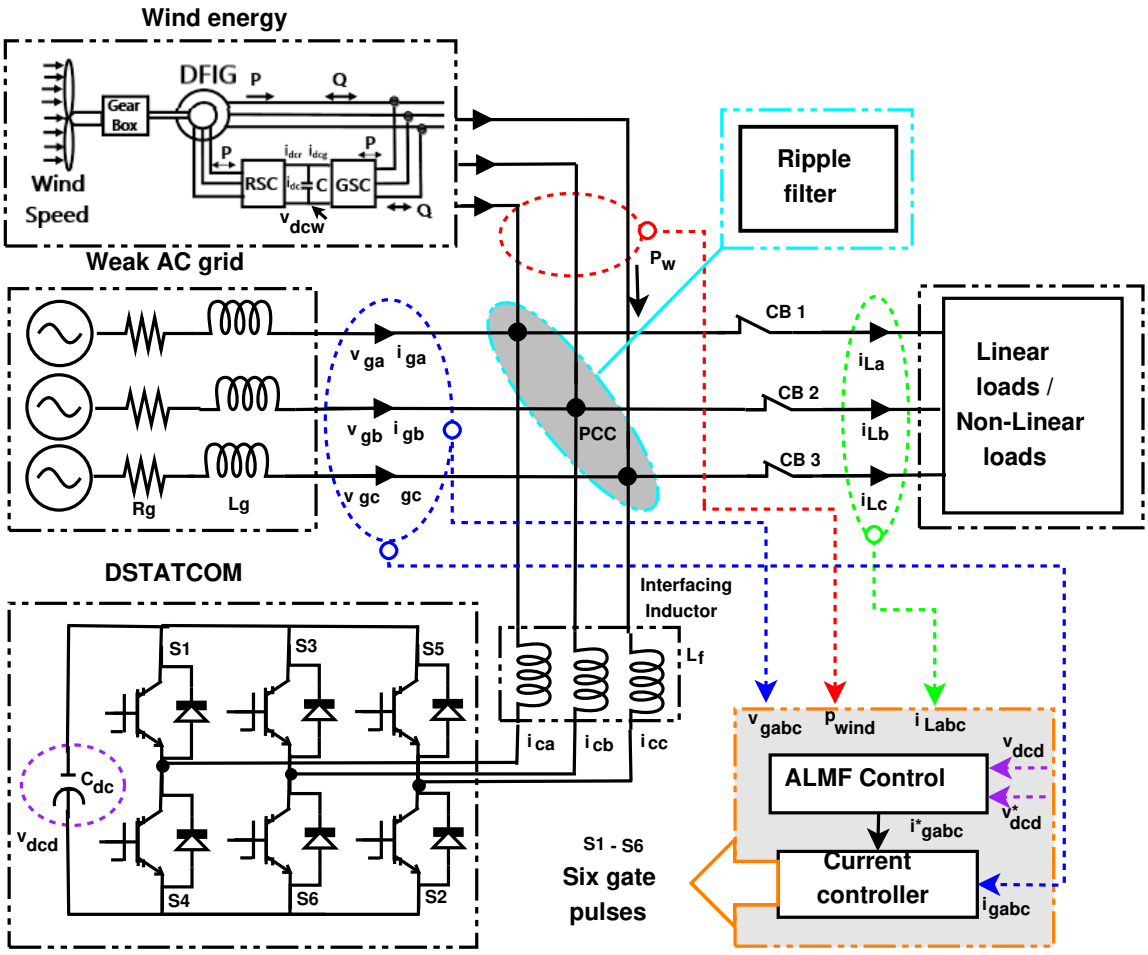

Figure 4.1: The system configuration of the rural grid.

Table 4.1: System parameters.

Parameters	MATALB simulation values	Experimental values
Type-III DFIG	1.5 MW,3 MW,4.5 MW,6 MW	0.400 kW
WE penetration level (25%)	4.5 MW, 575 V	0.400 kW, 415 V
Wind speed variations	15 m/s and 7.5 m/s	12 m/s and 7.2 m/s
SCR of grid	2.74, 5 and 7	2.74, 5 and 7
X/R ratio of grid	7	7
Step down transformer	0.575 kV / 0.415 kV	-
Linear loads at 0.8-lagging PF (100%)	18 MW	1.6 kW
Linear loads at 0.8-lagging PF (60%)	10.8 MW	0.960 kW
Rectifier based NL loads (40%)	7.2 MW	0.640 kW
DSTATCOM	4.5 MVAr, 680 Vdcd	5 kVAr, 500 Vdcd

4.4 DESIGNING OF ADAPTIVE LMF ALGORITHM

The design considerations of the basic and proposed adaptive LMF algorithm is explained in this subsection.

4.4.1 Standard Adaptive LMF Algorithm

The Least Mean Fourth (LMF) adaptive algorithm aims to identify the unknown coefficients vector adaptively by using the input signal $X(n)$ and the output $Y(n)$. The unknown system is shown in Fig. 4.2. In this system, the coefficients vector (W) of an N-length finite impulse response (FIR) filter and input signal vectors are defined as $W = [w_1, w_2, ..., w_N]^T$ and $X(n)$=$[x(n), x(n-1), ..., x(n-(N+1))]^T$, respectively. However, noise is represented by $Z(n)$, which is assumed to be independent with $X(n)$.

$$Y(n) = W^T \times X(n) + Z(n) \tag{4.1}$$

Let, $W(n)$ be the estimated coefficients-vector at n^{th} iteration. Similarly, the instantaneous error is express as $e(n) = Y(n) - W^T(n) \times X(n)$. The cost function $L_{lmf}(n)$ of standard LMF algorithm

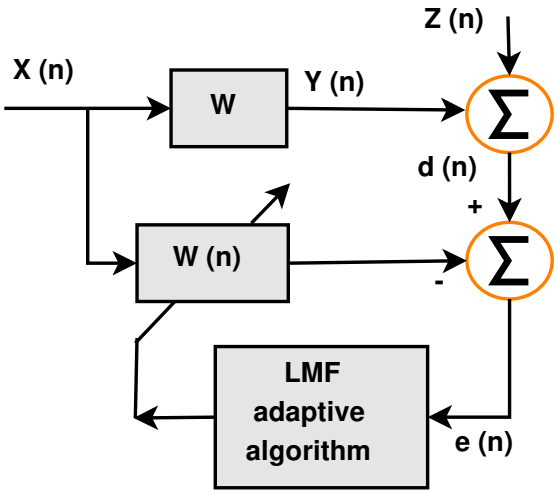

Figure 4.2: Weight updation in standard adaptive LMF algorithm.

is written as [Gui *et al.*, 2014]:

$$L_{lmf}(n) = 1/2(e^4(n)) \tag{4.2}$$

The coefficients-vector $W(n)$ is updated using LMF equation,

$$W(n+1) = W(n) - \tau(\partial L_{lmf}(n)/\partial W(n)) \tag{4.3}$$

$$W(n+1) = W(n) + \tau \times e^3(n) \times X(n) \tag{4.4}$$

The practical value of convergence factor (τ) varies between 0.01 to 1.0. The selection of optimal value increases the accuracy and the rate of convergence. Higher the value of τ, the rate of convergence is increased but at the cost of accuracy. Low value of τ gives good accuracy but the rate of convergence is slow [Haykin, 2008].

4.4.2 Proposed Adaptive LMF Control Algorithm

The block diagram of weight estimation using the adaptive Least Mean Fourth (ALMF) algorithm is as presented in Fig. 4.3. It can be observed that weights are estimated and updated after every iteration. The error signal ($e(n)$) is calculated using load current ($i_L(n)$), weight component ($w(n)$), and grid voltage unit templates ($u_t(n)$). Block diagram of the adaptive Least Mean Fourth (ALMF) control algorithm is illustrated in Fig. 4.4. The proposed adaptive control algorithm adapts the multiple changes related to WE penetration into the weak grid according to the system behaviour by adjusting the system weights. This algorithm works on continuously updating the weight component according to the system data. The process involved to estimate reference grid currents and gating signals for the DSTATCOM is detailed below.

1. **Computation of active and reactive voltage unit templates** Three-phase grid voltage are utilized to compute terminal voltage (v_t), active and reactive voltage unit templates,

$$v_t = \sqrt{2/3(v_{ga}^2 + v_{gb}^2 + v_{gc}^2)} \tag{4.5}$$

$$u_{tpabc} = v_{gabc}/v_t \tag{4.6}$$

$$\left\{\begin{array}{c} u_{tqa} = -u_{tpb}/\sqrt{3} + u_{tpc}/\sqrt{3} \\ u_{tqb} = \sqrt{3}u_{tpa}/2 + (u_{tpb} - u_{pc})/2\sqrt{3} \\ u_{tqc} = -\sqrt{3}u_{tpa}/2 + (u_{tpb} - u_{pc})/2\sqrt{3} \end{array}\right\} \tag{4.7}$$

2. **Computation of active and reactive loss components** The PI voltage controller maintains terminal voltage at PCC by generating reactive loss component (W_{cq}). This W_{cq} is used to regulate AC voltage at n^{th} sampling instant,

$$W_{cq}(n+1) = W_{cq}(n) + k_{pq}(v_{te}(n+1) - v_{te}(n)) + k_{iq}v_{te}(n+1) \tag{4.8}$$

$W_{cq}(n+1)$ is updated reactive loss component and $v_{te}(n+1)$ is updated voltage error. However, the present value of this voltage error (v_{te}) is,

$$v_{te}(n) = v_{tn}(n) - v_t(n) \tag{4.9}$$

The correct estimation of DC-link voltage is necessary for minimizing the voltage fluctuations during the high penetration of active power at PCC. Therefore, the PI controller has tuned with the optimum value of proportional $K_{pd} = 0.25$ and integral $K_{id} = 0.25$ gains. This controller generates an active loss component ($W_{cp)}$ for maintaining the dc-bus voltage at n^{th} sampling instant,

$$W_{cp}(n+1) = W_{cp}(n) + k_{pd}(v_{de}(n+1) - v_{de}(n)) + k_{id}v_{de}(n+1) \tag{4.10}$$

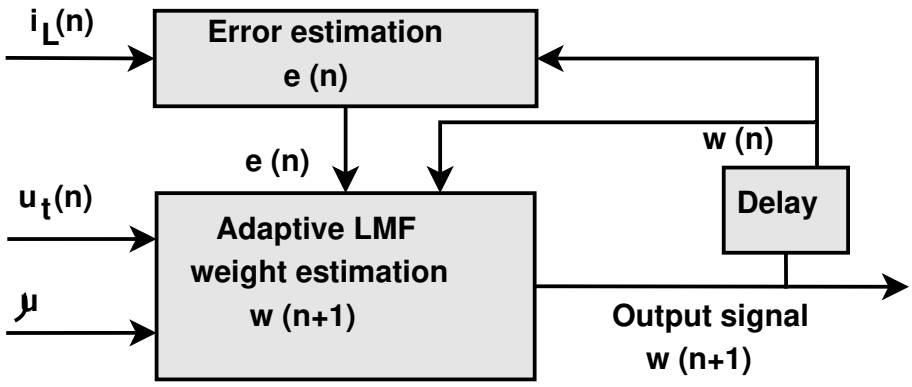

Figure 4.3: Block diagram of weight estimation using the adaptive LMF algorithm.

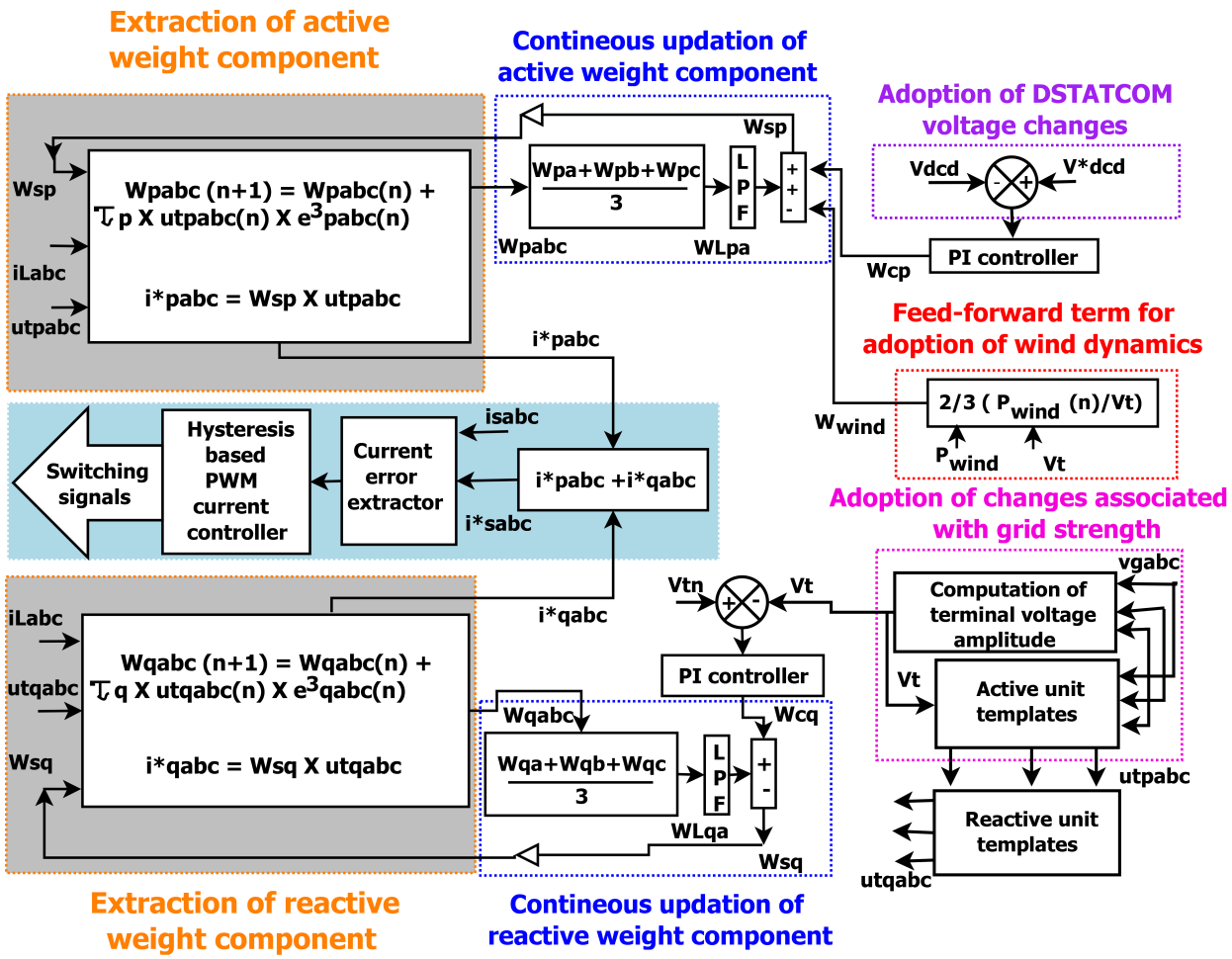

Figure 4.4: Block diagram of proposed adaptive LMF control algorithm.

Where, $W_{cp}(n+1)$ is updated active loss component and $v_{de}(n+1)$ is updated DC voltage error. However, the current value of voltage error (v_{de}) is computed using the DC-bus reference voltage (v^*_{dcd}), which is computed in equation (2.46).

$$v_{de}(n) = v^*_{dcd}(n) - v_{dcd}(n) \tag{4.11}$$

However, the reference DC bus voltage of DSTATCOM is calculated as,

$$(v^*_{dcd} = 2\sqrt{2}v_{LL}/\sqrt{3}m) \tag{4.12}$$

v_{LL} is represent voltage (line to line) at POC and m is modulation index. The stability investigation of the system is carried out for DSTATCOM DC-bus control using the Bode stability plot. The transfer function $G_S(s)$ is written as [Agarwal *et al.*, 2017a] :

$$G_s(s) = G_p(s) \times G_c(s) = [(1/sc_{dc}) \times (k_p + k_i/s)] \tag{4.13}$$

where, G_p(s) and G_c(s) are the transfer functions of the plant and PI voltage controller. It can be seen from Fig 4.5 that the system is stable with a phase margin in a stable region.

3. **Computation of feed-forward term of WE source** Wind-feed-forward term (W_{wind}) is implemented in the algorithm to adapt the changes associated with WE penetration. It is calculated using the current output power (P_{wind}) of WE.

$$W_{wind}(n) = 2P_{wind}(n)/3v_t \tag{4.14}$$

4. **Computation of active, reactive weight and error components of load current** The active and reactive weight components of three-phase load currents are computed as,

$$w_{pabc}(n+1) = w_{pabc}(n) + \tau_p \times u_{pabc}(n) \times e^3_{pabc}(n) \tag{4.15}$$

$$w_{qabc}(n+1) = w_{qabc}(n) + \tau_q \times u_{qabc}(n) \times e^3_{qabc}(n) \tag{4.16}$$

where, $W_{pabc}(n+1)$ are updated 3-phase active weight components of load current, The $u_{pabc}(n)$ and $u_{qabc}(n)$ are active and quadrature unit templates of weak grid. The convergence factors (τ_p and τ_q) are selected 0.2. The active ($e^3_{pabc}(n)$) and reactive ($e^3_{qabc}(n)$) error components are estimated as,

$$e_{pabc}(n) = i_{Labc}(n) - u_{pabc}(n) \times w_{pabc}(n) \tag{4.17}$$

$$e_{qabc}(n) = i_{Labc}(n) - u_{qabc}(n) \times w_{qabc}(n) \tag{4.18}$$

Where, $i_{Labc}(n)$ load currents, $w_{pabc}(n)$ and $w_{qabc}(n)$ are the present value of the active and reactive weight component.

5. **Computation of total active, reactive weight components** The total active weight component (W_{sp}) is computed by combining the dc loss component (W_{cp}) to the average active weight component (W_{Lpa}) and then deducted using the wind feed-forward weight (W_{wind}). The averaging of the weight components are minimized the unbalancing in the system.

$$W_{sp} = W_{Lpa} + W_{cp} - W_{wind} \tag{4.19}$$

$$W_{Lpa} = (W_{pa} + W_{pb} + W_{pc})/3 \tag{4.20}$$

Likewise, the total reactive weight component (W_{sq}) is estimated by deducting the average reactive weight component (W_{Lqa}) to the ac loss component (W_{cq}),

$$W_{sq} = W_{cq} - W_{Lqa} \tag{4.21}$$

$$W_{Lqa} = (W_{qa} + W_{qb} + W_{qc})/3 \tag{4.22}$$

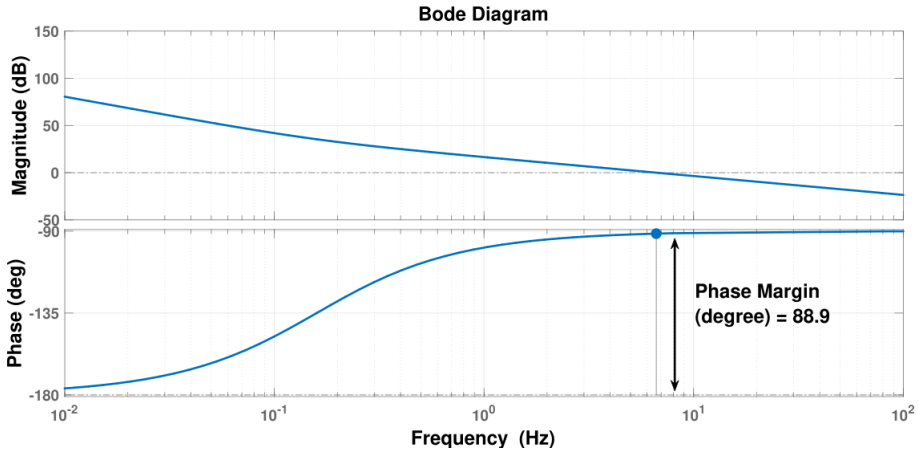

Figure 4.5: Bode stability diagram of ALMF using controller inputs.

6. **Computation of reference current signals** The total active and reactive weight component (W_{sp} and W_{sq}) are multiplied with the active and reactive unit voltage templates to generate the i^*_{pabc} and i^*_{qabc} reference grid currents, The active reference signal (i^*_{pabc}) is estimated using total active weight component (W_{sp}) and 3-phase active unit templates.

$$i^*_{pabc} = W_{sp} \times u_{tpabc} \tag{4.23}$$

Similarly, the reactive reference signal (i^*_{qabc}) is estimated using reactive weight component (W_{sq}) and 3-phase active unit templates.

$$i^*_{qabc} = W_{sq} \times u_{tqabc} \tag{4.24}$$

Three-phase reference grid currents (i^*_{gabc}) are generated by combining active reference signal (i^*_{pabc}) and reactive reference signal (i^*_{qabc}).

$$i^*_{gabc} = i^*_{pabc} + i^*_{qabc} \tag{4.25}$$

7. **Generation of Switching Signals** The hysteresis current controller (HCC) is utilized to generate six-gating signals for DSTATCOM switches, where 3-phase estimated grid signals (i^*_{gabc}) are compared with the sensed weak grid signal (i_{gabc}). In this context two logics are employed, If (i_{gabc}) > ($i^*_{gabc} + hcb$), the lower switch is OFF and the upper switch is ON. If (i_{gabc}) < ($i^*_{gabc} - hcb$), the upper switch is OFF and the lower switch is ON.

4.5 SIMULATION RESULTS AND DISCUSSIONS

The performance of the proposed methodology has been demonstrated by simulating unbalance with various strength of grid, different composition of the loads and various penetration levels. The details of the case studies are present in Table 4.2.

4.5.1 Case-1: Enhancement of Wind Penetration Levels

The penetration levels are enhanced from 10% to 30% into the grid of SCR 2.74 with 100% linear load. Figure 4.6 presents the 30% WE penetration level with its voltage. It can be found that the power quality of the system in terms of voltage is maintained within the stability range

Table 4.2: Parameter variations for various case studies.

S.No.	Parameters	Parameter Variations	
		Simulation	Experimental
1	SCR	2.74 to 7	2.74 to 7
2	Load-1	100% 0.8 lag-PF load	100% 0.8 lag-PF load
3	Load-2	Unbalanced 40% NL load, 60% linear load	Unbalanced 40% NL load, 60% linear load
4	WE Penetration levels	10%, 18%, 25% and 30%	10%, 18%, 25% and 30%
5	Wind speed variation	15m/s to 7.5 m/s	12 m/s to 7.2 m/s
6	Synchronization point	at 1 second	at 1 second

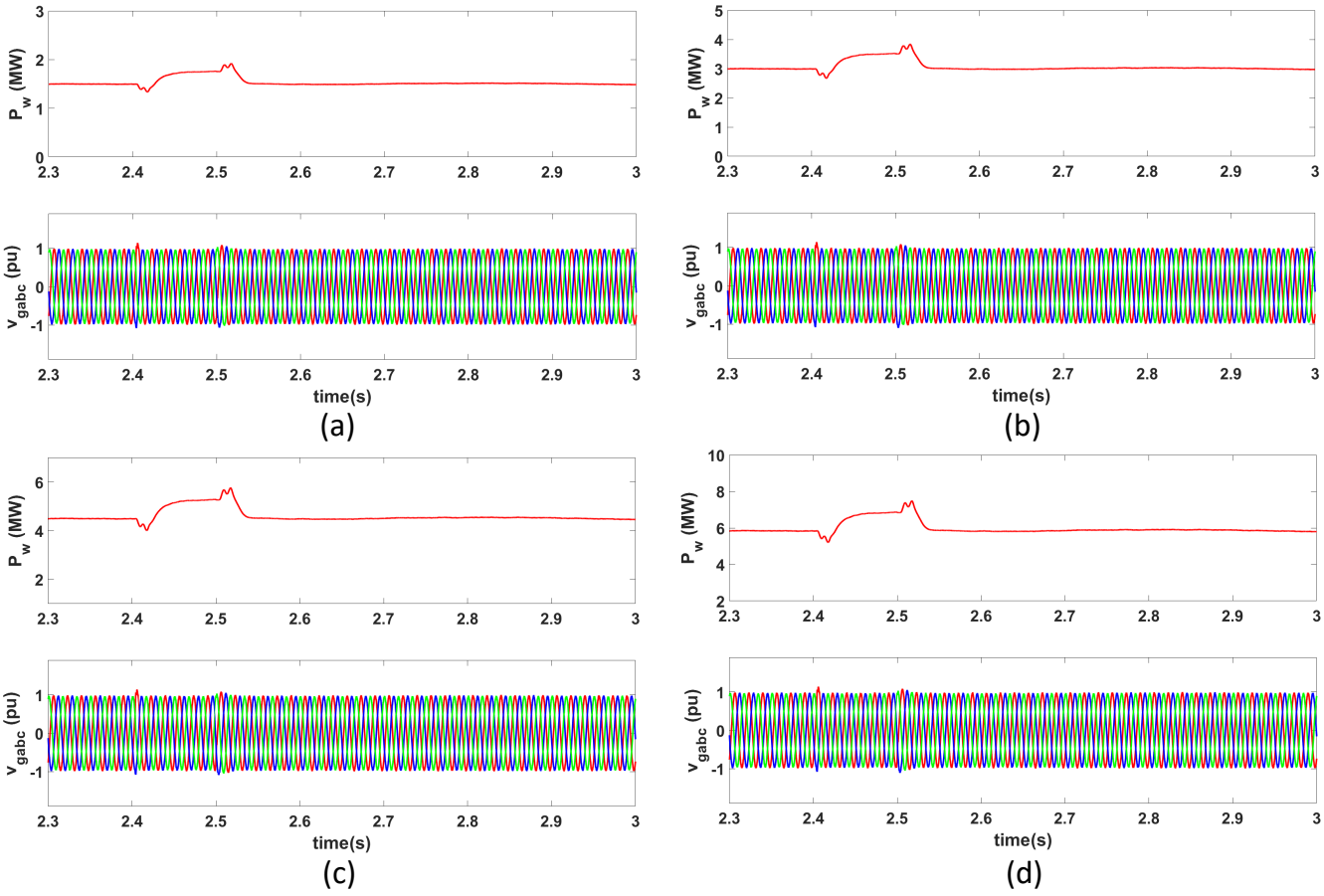

Figure 4.6: WE penetration levels with 100% linear load (a) 10%, (b) 18%, (c) 25%, (d) 30%.

(*i.e.* $\pm 10\%$) up to30% WE penetration level. However, up to 25%, the active power of WE sources is tracked with more than 99% accuracy, and beyond 25%, the wind power tracking accuracy is deteriorated due to PQ issues. The simulation results are shown in Table 4.3. It is found that increments in the penetration level up to 30% harmonic levels also increase in the system. These harmonic levels are well maintained under the international PQ standards. The power factor, the magnitude of voltage and harmonic levels of voltage and current of the grid are observed to meet PQ standards with increments in the penetration level. It has also been observed that the presence of non-linear load also deteriorates the PQ and limit the wind energy penetration levels.

Table 4.3: Enhancement of WE penetration levels (Simulation).

Penetration levels (↓)	Loads (→)	Load-1		
	SCR (→)	2.74	5	7
	Simulation analysis			
10%	v_{gTHD}	2.19	2.11	2.07
	i_{gTHD}	0.17	0.14	0.10
	PF_g	1	1	1
	P_w (MW)	1.5	1.5	1.5
	Q_d (MVAr)	0.48	0.48	0.47
	v_g (Volt)	419.9	417.11	417.2
18%	v_{gTHD}	2.34	2.31	2.25
	i_{gTHD}	0.44	0.41	0.36
	PF_g	0.99	0.99	1
	P_w (MW)	3	3	3
	Q_d (MVAr)	0.65	0.65	0.64
	v_g (Volt)	419.11	417.13	417.1
25%	v_{gTHD}	2.6	2.53	2.48
	i_{gTHD}	0.93	0.84	0.81
	PF_g	0.99	0.99	0.99
	P_w (MW)	4.5	4.5	4.5
	Q_d (MVAr)	0.77	0.77	0.76
	v_g (Volt)	419.15	417.15	417.1
30%	v_{gTHD}	4.39	4.24	4.14
	i_{gTHD}	2.79	2.52	2.43
	PF_g	0.91	0.91	0.91
	P_w (MW)	5.56	5.56	5.56
	Q_d (MVAr)	1.46	1.46	1.44
	v_g (Volt)	421.4	420.3	420.1

4.5.2 Case-2: Performance with NL Load at Rated Wind Speed

Fig. 4.7 presents the various waveforms of the proposed method for mitigating the PQ in a grid with an SCR of 2.74. The load combination is 40% NL load + 60% linear load, and WE penetration is 25%. An unbalance simulated from 2.4 to 2.5-second by disconnecting phase-a load and connecting it back. Fig. 4.7 (a) shows the updating and recovery stage (2.49 to 2.53-second). During load unbalancing, the rapid compensating current (i_{cabc}) has been added by the DSTATCOM to maintain grid voltage and to compensate for the unbalance. The grid current (i_{gabc}), voltage (v_{gabc}), wind current (i_{wabc}) and wind voltage (v_{wabc}) are continued to be balanced and sinusoidal. The DC-link voltage (v_{dcd}) of the DSTATCOM has been maintained at a reference value with fewer fluctuations, illustrating the proposed adaptive algorithm's effectiveness.

Figure 4.7 (b) shows that, DSTATCOM continuous to inject reactive power (Q_d = 0.85 MVAr) to maintained the rated active power of the wind (P_w = 4.5 MW) by keeping wind voltage (v_w) within voltage stability range. The DC-link voltage of the wind side converter (V_{dcw}) is maintained to reference voltage (i.e. 1150 V). It has also been illustrated that the rural grid's reactive power (Q_g) requirement is increased during unbalancing, which was effectively compensated by the proposed method and maintained the active power of grid (P_g) constant without any fluctuations.

The intermediate signals computed in the ALMF control algorithm is illustrated in Fig.

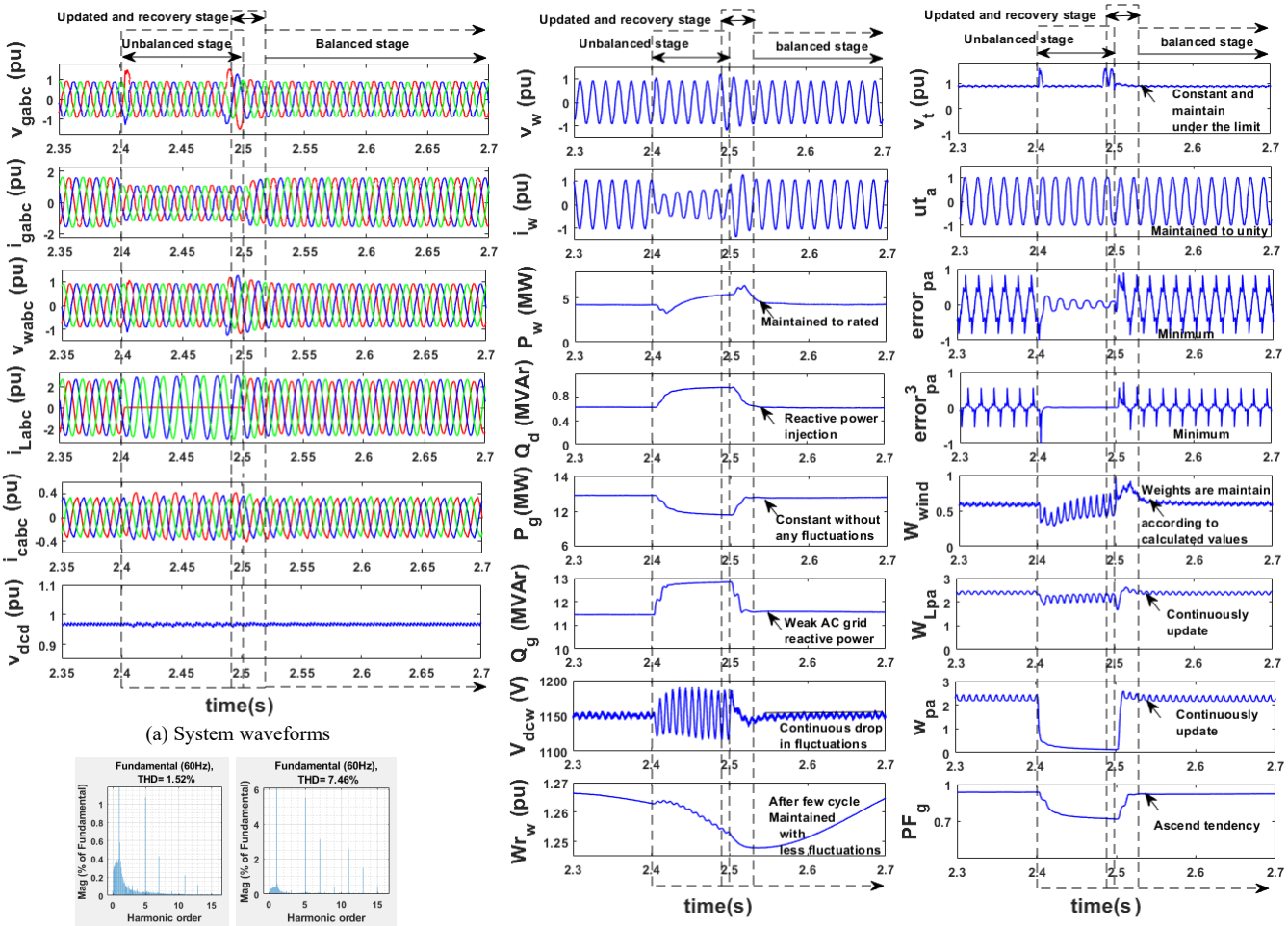

(a) System waveforms

(b) Grid current and voltage harmonics

(c) Wind and grid signals

(d) Intermediate signals

Figure 4.7: Performance of proposed method with NL load at rated wind speed.

4.7 (c). The terminal voltage (v_t) at PCC is found to be within the voltage stability limit (i.e. 0.9 pu - 1.10 pu) by keeping unit templates (u_{ta}) of rural grid unity. The power factor (PF_g), harmonics levels of the grid are maintained as per the PQ standards. The adaptive least mean fourth current error ($error^3_{pa}$) is found to be minimal compared to the least mean square current error ($error_{pa}$). The simulated wind feed-forward weight component (W_{wind}) has been found similar to the calculated W_{wind}. Likewise, the average active weight (W_{Lpa}) and active weight component (w_{pa}) have been visualized continuously updated to minimize the recovery time and stable the system with lesser time.

4.5.3 Case-3: Performance with NL Load at Minimum Wind Speed

This case study discusses PQ and high WE penetration with wind speed below its rated speed under the grid SCR of 2.74 and load combination of 40% NL load + 60% linear load. The wind speed has been decreased from a rated speed of 15 m/s to a minimum wind speed of 7.5 m/s at 3.5-second. Fig. 4.8 (a),(b) shows that, the grid voltage, unit templates (ut_a), and current error ($error^3_{pa}$) signals are found to be stable without change. The magnitude of terminal voltage (v_t), dc-link voltage of DSTATCOM (v_{dcd}) and wind (V_{dcw}) are maintained to their reference value with less fluctuations due to controlled action of proposed algorithm. Meanwhile, the wind output power (P_w), grid current and reactive power (Q_d) of DSTATCOM are decreased with WE rotor speed (Wr_w). The grid current and voltage harmonics are found to be 1.93% and 4.43%, respectively.

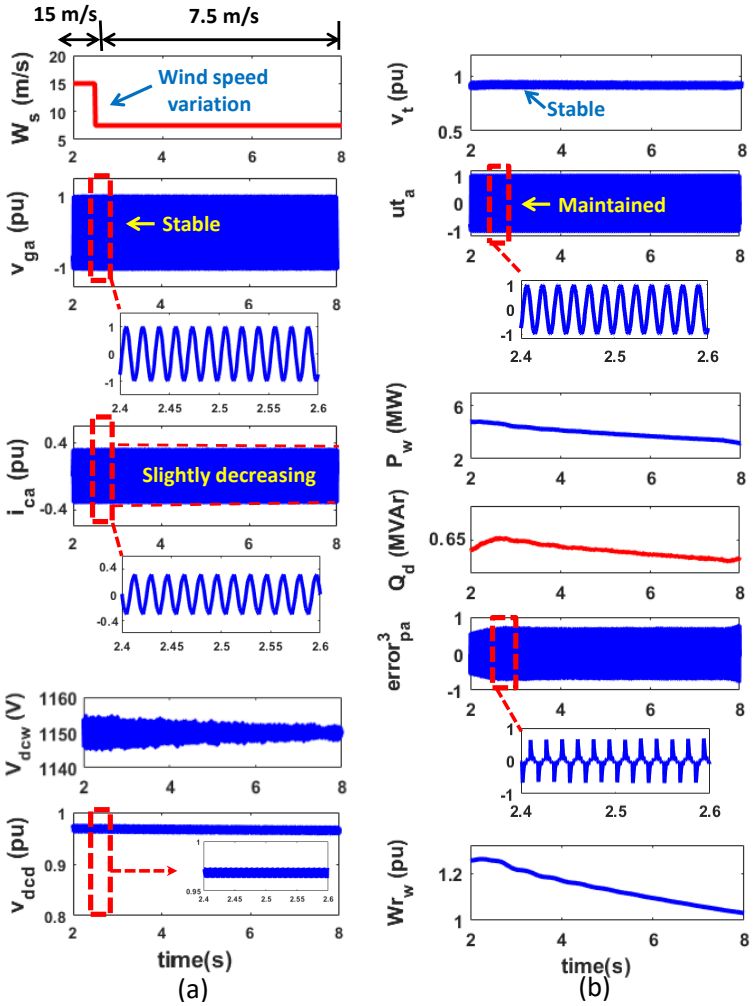

Figure 4.8: Performance of proposed method with NL load at minimum wind speed.

4.5.4 Case-4: Effect of Variation in Grid SCR

The proposed method has been examined for unbalanced studies by varying the SCR from 2.74-7 under different load compositions. It can be observed from Table 4.4 that the DSTATCOM injects reactive power (Q_d) at the PCC to maintained the active power of the wind (P_w), grid voltage (v_g), harmonic levels (v_{gTHD} and i_{gTHD}) and power factor (PF_g). The variations in the SCR values from 2.74-7 illustrated that slight changes are observed in the second and third decimal harmonics values. No significant disagreement was observed, and results show no adverse effect on the system with the varying grid strength.

This can also be verified through the stability analysis of the system is carried out for various strengths of the grid using the Bode stability plot. The transfer function $T_g(s)$ for various short circuit ratios of the grid using grid impedance and controller input gains is written as:

$$T_g(s) = T_p(s) \times T_c(s) = \left[\frac{1}{sZ_g} \times (k_p + \frac{k_i}{s})\right] \tag{4.26}$$

T_p(s); Plant transfer function, T_c(s); PI transfer function and Z_g: grid impedance of different SCRs. Fig. 4.9 shows that the stability of the system is degraded with a grid SCR of 1 due to large impedance, and performance is observed as unsatisfactory. The phase margin of grid impedance's of SCR-2.74 and SCR-7 are located in the stable region, indicating that the SCR of 2.74 and beyond the system is stable.

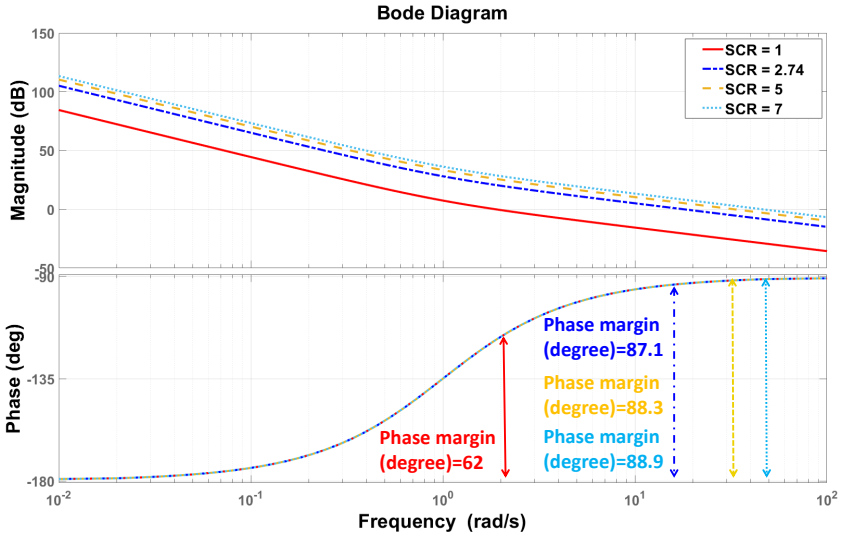

Figure 4.9: Bode stability plot for various grid SCR using grid impedance and controller inputs.

Table 4.4: Performance under variation in grid SCR (Simulation).

Penetration levels (↓)	Loads (→)	Load-1			Load-2		
	SCR (→)	2.74	5	7	2.74	5	7
		Simulation analysis					
10%	v_{gTHD}	2.19	2.11	2.07	4.38	4.29	4.21
	i_{gTHD}	0.17	0.14	0.10	1.33	1.29	1.21
	PF_g	1	1	1	0.98	0.98	1
	P_w (MW)	1.5	1.5	1.5	1.5	1.5	1.5
	Q_d (MVAr)	0.48	0.48	0.47	0.56	0.56	0.55
	v_g (Volt)	419.9	417.11	417.2	419.9	417.7	416.2
18%	v_{gTHD}	2.34	2.31	2.25	5.0	4.95	4.86
	i_{gTHD}	0.44	0.41	0.36	1.45	1.41	1.34
	PF_g	0.99	0.99	1	0.98	0.98	1
	P_w (MW)	3	3	3	3	3	3
	Q_d (MVAr)	0.65	0.65	0.64	0.74	0.74	0.73
	v_g (Volt)	419.11	417.13	417.1	419.17	417.13	417.3
25%	v_{gTHD}	2.6	2.53	2.48	7.46	7.43	7.37
	i_{gTHD}	0.93	0.84	0.81	1.30	1.09	1.02
	PF_g	0.99	0.99	0.99	0.98	0.98	0.98
	P_w (MW)	4.5	4.5	4.5	4.5	4.5	4.5
	Q_d (MVAr)	0.77	0.77	0.76	0.85	0.84	0.83
	v_g (Volt)	419.15	417.15	417.1	419.15	417.15	417.4
30%	v_{gTHD}	4.39	4.24	4.14	8.78	8.60	8.23
	i_{gTHD}	2.79	2.52	2.43	4.56	4.51	4.36
	PF_g	0.91	0.91	0.91	0.89	0.89	0.89
	P_w (MW)	5.56	5.56	5.56	5.53	5.53	5.53
	Q_d (MVAr)	1.46	1.46	1.44	1.61	1.61	1.59
	v_g (Volt)	421.4	420.3	420.1	598	597.9	597.98

4.5.5 Case-5: Synchronization of DFIG with Rural Grid

The waveforms obtained using the ALMF algorithm for soft synchronization of DFIG into the weak grid (SCR=2.74) at 25% WE penetration are similar to those obtained using the ADALINE-LMS. The WE source and DSTATCOM are connected at 1-second and found that <0.9-s is needed for maintaining soft synchronization. Table 4.7 shows the PQ analysis under the synchronization of DFIG with the rural grid. The observed weak grid, transient (transition) and steady-state (stable) stages voltage and current harmonics are 13.1%, 14.21%, 7.51% and 7.3%, 4.14%, 1.3%, respectively.

4.6 EXPERIMENTAL RESULTS AND DISCUSSIONS

The experimental prototype is depicted in Fig 4.10. The developed prototype consists of SEMIKRON makes VSC based DSTATCOM, and Lucas-Nulle makes a DFIG based WE emulator. The grid currents and voltage signals and the dc-link voltage of DSTATCOM are sensed using Hall effect based TI-TMCS1100 sensors. The execution of the control algorithm is carried out on DSP (dSPACE-1104). Switching signals are amplified using the buffer-circuit (Microchip-TC427). Tektronix DPO4104B and YOKOGAWA-WT3000 are used to record the waveforms and PQ, respectively. The detailed specifications of the system used for Experimental validation are presented in Table 4.1.

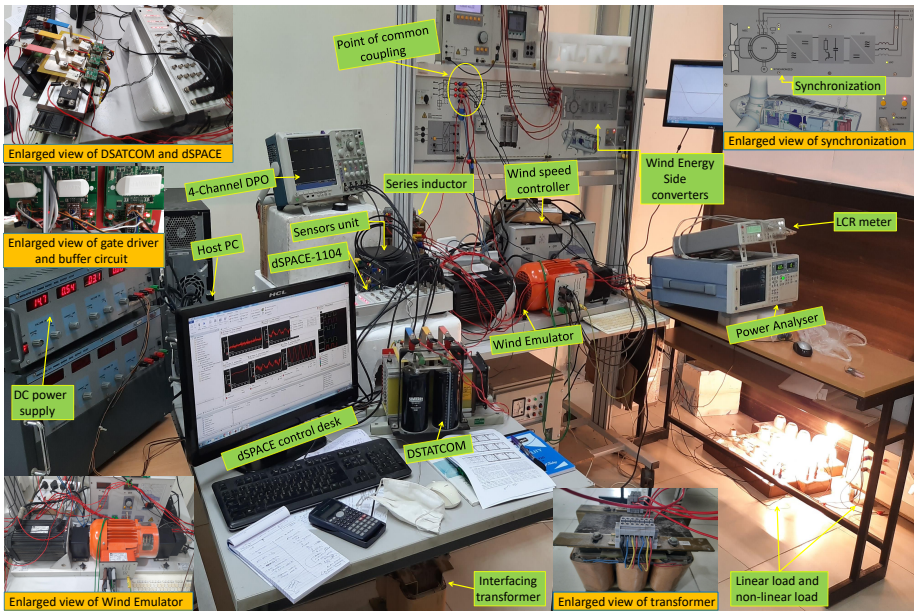

Figure 4.10: Laboratory-based experimental prototype.

4.6.1 Case-1: Enhancement of Wind Penetration Levels

The penetration levels are enhanced from 10% to 30% into the grid of SCR 2.74 with 100% linear load. Figure 4.11 presents the 30 % WE penetration level with its voltage. It can be found that the power quality of the system in terms of voltage is maintained within the stability range (*i.e.* $\pm 10\%$) up to 25% WE penetration level. However, up to 25%, the active power of WE sources is tracked with more than 99% accuracy, and beyond 25%, the wind power tracking accuracy is deteriorated due to PQ issues. The experimental results are shown in Table 4.5. It is found that increments in the penetration level up to 30% harmonic levels also increase in the system. These

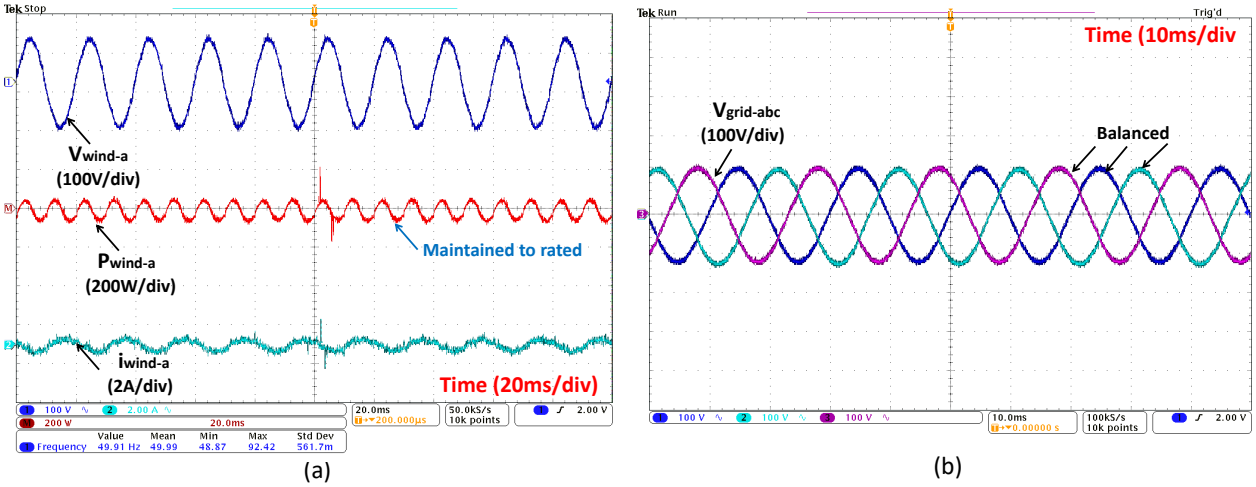

Figure 4.11: WE penetration level with 100% linear load (a) Active power, (b) Grid voltage.

Table 4.5: Enhancement of WE penetration levels (Experimental).

Penetration levels (↓)	Loads (→)	Load-1		
	SCR (→)	2.74	5	7
	Experimental analysis			
10%	v_{gTHD}	2.39	2.35	2.2
	i_{gTHD}	0.32	0.30	0.25
	PF_g	1	1	1
	P_w (kW)	0.279	0.279	0.279
	Q_d (kVAr)	0.057	0.057	0.056
	v_g (Volt)	417.5	416.5	416.1
18%	v_{gTHD}	2.79	2.71	2.64
	i_{gTHD}	1.03	0.95	0.86
	PF_g	0.99	0.99	0.99
	P_w (kW)	0.279	0.279	0.279
	Q_d (kVAr)	0.063	0.063	0.062
	v_g (Volt)	417.9	416.11	416.3
25%	v_{gTHD}	3.13	3.01	2.97
	i_{gTHD}	1.30	1.09	1.02
	PF_g	0.99	0.99	0.99
	P_w (kW)	0.279	0.279	0.279
	Q_d (kVAr)	0.075	0.075	0.073
	v_g (Volt)	417.7	416.6	416.05
30%	v_{gTHD}	3.13	4.82	4.73
	i_{gTHD}	3.9	3.27	3.06
	PF_g	0.9	0.9	0.9
	P_w (kW)	0.279	0.279	0.279
	Q_d (kVAr)	0.144	0.144	0.142
	v_g (Volt)	420.7	419.4	419.01

harmonic levels are well maintained under the international PQ standards. The power factor, the magnitude of voltage and harmonic levels of voltage and current of the grid are observed to meet

PQ standards with increments in the penetration level. It has also been observed that the presence of non-linear load also deteriorates the PQ and limit the wind energy penetration levels.

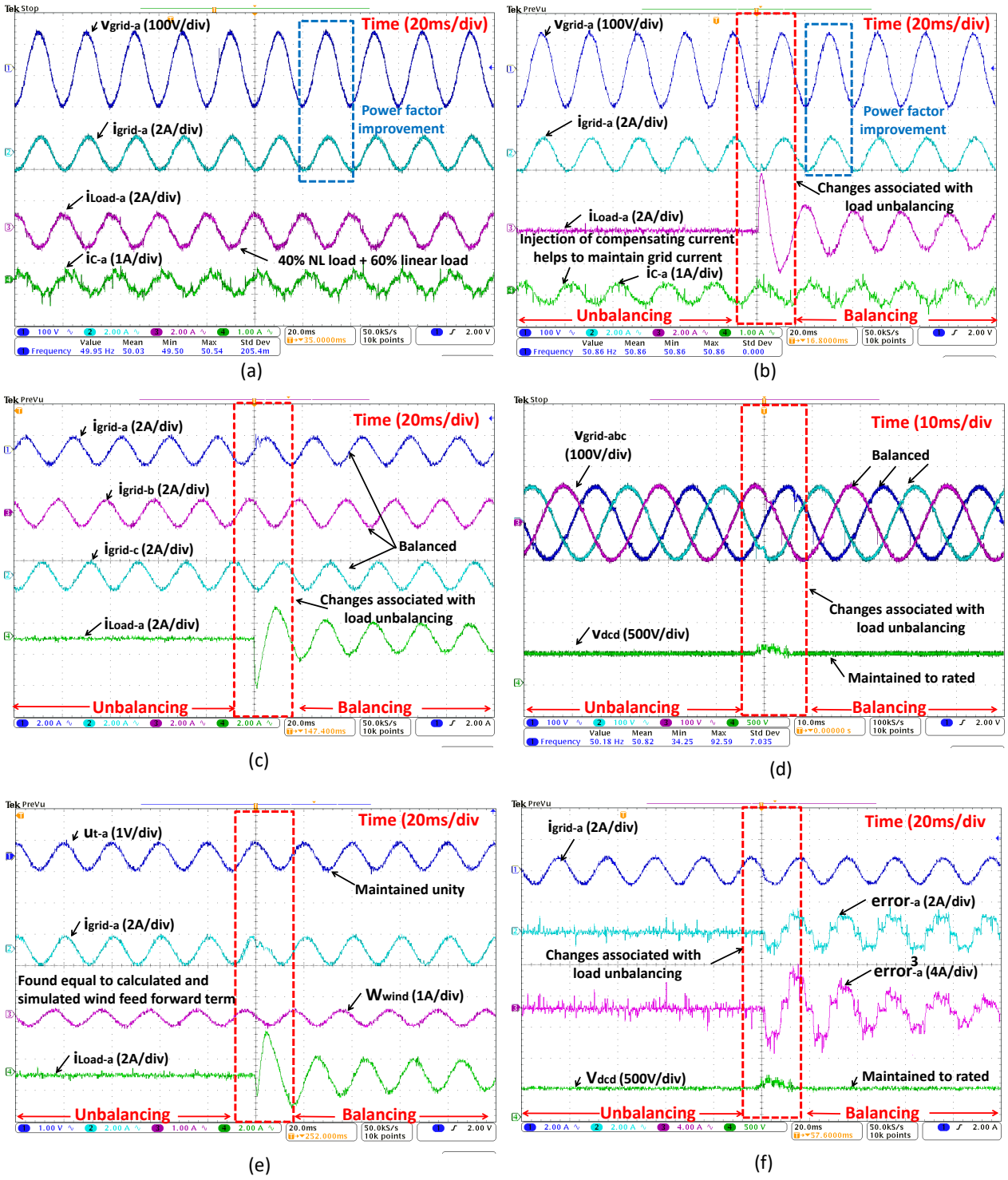

Figure 4.12: Performance of proposed method at rated wind speed (a) With balanced NL load, (b),(c),(d),(e),(f) With unbalanced NL load.

4.6.2 Case-2: Performance with NL Load at Rated Wind Speed

The WE source is integrated at PCC with the SCR of 2.74 under the rated wind speed ($12m/s$) in the presence of 40% NL load + 60% linear load. Figure 4.12 (a) shows the response of the system using the proposed method. The DSTATCOM adds the compensating current (i_{C-a}) to maintain grid voltage (v_{grid-a}), and current (i_{grid-a}) balanced and sinusoidal in the presence of balanced non-linear load.

Fig 4.12 (b) illustrated the rapid compensating current added by the DSTATCOM to maintain grid voltage and to compensate for the unbalance in the grid current. The steady-state error in the amplitudes of grid current is found to be 0.013 A. During the load unbalance, the compensating current is observed non-sinusoidal due to the harmonics in the wind current. The three-phase grid current and voltage ($v_{grid-abc}$) are observed sinusoidal and balanced in Fig 4.12 (c) and (d).

The intermediate signals computed in ALMF control is as illustrated in Fig 4.12 (e), (f). Figure 4.12 (e) shows that the unit voltage template (u_{t-a}) is kept unity and the calculated, simulated and experimentally observed wind feed-forward term ($W_{wind} \sim 0.65A$) are matched, which shows the proposed method's efficacy and applicability at remote grids. The least mean fourth current error ($error_{pa}^{3}$) is found to be minimal compared to the least mean square current error ($error_{pa}$). The DC-link voltage (v_{dcd}) of the DSTATCOM is maintained at its reference value.

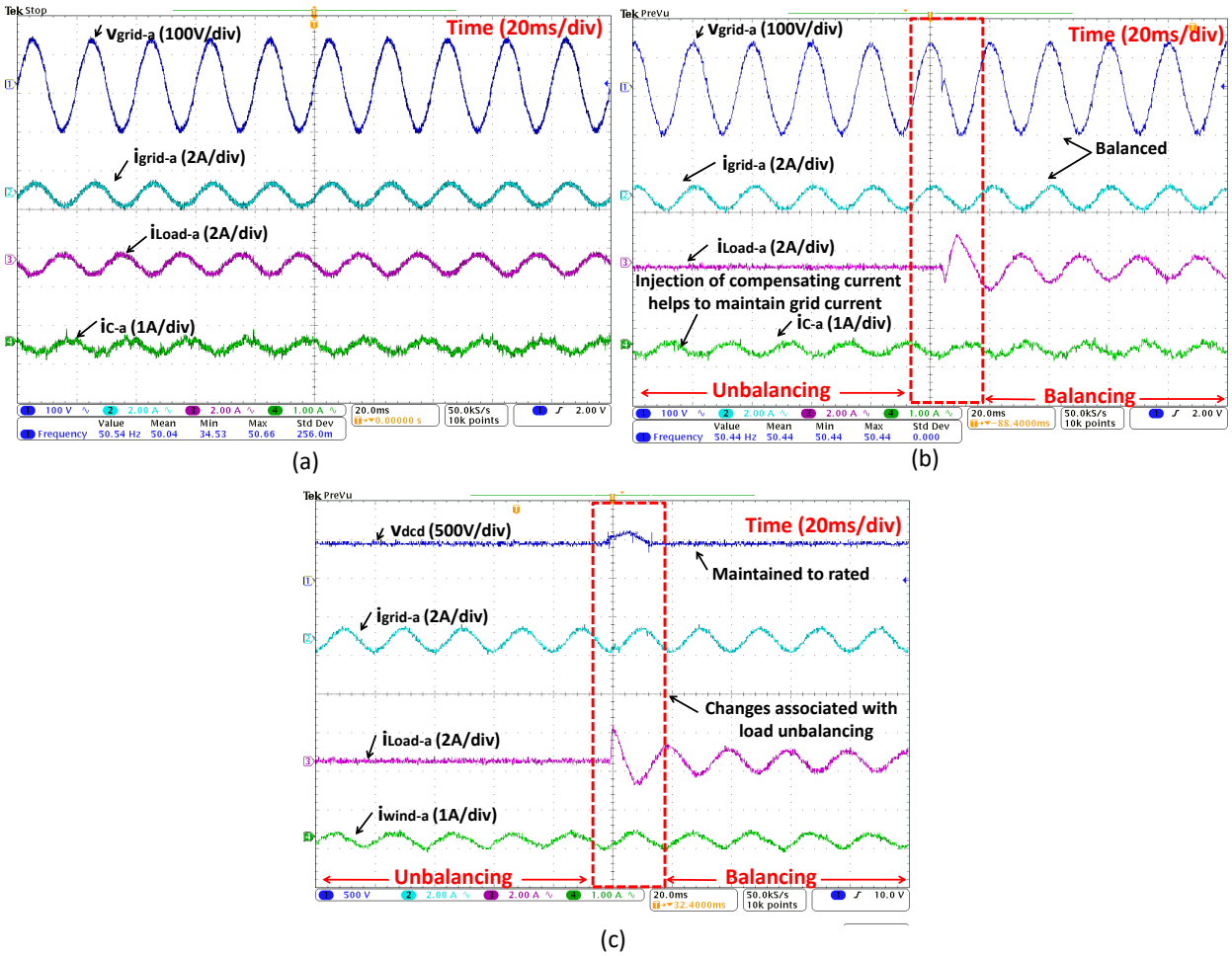

Figure 4.13: Performance of proposed method at minimum wind speed. (a) With balanced NL load, (b),(c) With unbalanced NL load.

4.6.3 Case-3: Performance with NL Load at Minimum Wind Speed

Similar case studies have been performed with the minimum wind speed ($7.2m/s$). The grid and WE signals are depicted in Fig 4.13 (a)-(c). It has been observed from the results that grid voltage (v_{grid-a}) is maintained under the voltage stability limit. The DC-link voltage (v_{dcd}) of the DSTATCOM is found to be stable. However, the amplitudes of the grid (i_{grid-a}) and wind (i_{wind-a}) current are found less than those obtained with rated speed wind signals. The harmonics of voltage and current are found to be 4.82% and 2.17%, respectively.

4.6.4 Case-4: Effect of Variation in Grid SCR

The proposed method has been examined for unbalanced studies by varying the SCR from 2.74-7 under different load compositions. It can be observed from Table 4.6 that the DSTATCOM injects reactive power (Q_d) at the PCC to maintained the active power of the wind (P_w), grid voltage (v_g), harmonic levels (v_{gTHD} and i_{gTHD}) and power factor (PF_g). The variations in the SCR values from 2.74-7 illustrated that slight changes are observed in the second and third decimal harmonics values. No significant disagreement was observed, and results show no adverse effect on the system with the varying grid strength.

Table 4.6: Performance under variation in grid SCR (Experimental).

Penetration levels (↓)	Loads (→)	Load-1			Load-2		
	SCR (→)	2.74	5	7	2.74	5	7
		Experimental analysis					
10%	v_{gTHD}	2.39	2.35	2.2	4.70	4.57	4.31
	i_{gTHD}	0.32	0.30	0.25	1.51	1.47	1.40
	PF_g	1	1	1	0.98	0.98	1
	P_w (kW)	0.279	0.279	0.279	0.279	0.279	0.279
	Q_d (kVAr)	0.057	0.057	0.056	0.0645	0.063	0.062
	v_g (Volt)	417.5	416.5	416.1	417.5	416.6	416.1
18%	v_{gTHD}	2.79	2.71	2.64	5.41	5.11	5.3
	i_{gTHD}	1.03	0.95	0.86	1.60	1.57	1.48
	PF_g	0.99	0.99	0.99	0.98	0.98	0.98
	P_w (kW)	0.279	0.279	0.279	0.279	0.279	0.279
	Q_d (kVAr)	0.063	0.063	0.062	0.087	0.086	0.085
	v_g (Volt)	417.9	416.11	416.3	417.9	416.7	416.2
25%	v_{gTHD}	3.13	3.01	2.97	7.69	7.57	7.51
	i_{gTHD}	1.30	1.09	1.02	1.95	1.82	1.76
	PF_g	0.99	0.99	0.99	0.98	0.98	0.98
	P_w (kW)	0.279	0.279	0.279	0.279	0.279	0.279
	Q_d (kVAr)	0.075	0.075	0.73	0.108	0.1065	0.104
	v_g (Volt)	417.7	416.6	416.05	417.7	416.6	417.15
30%	v_{gTHD}	3.13	4.82	4.73	9.41	9.15	8.97
	i_{gTHD}	3.9	3.27	3.06	5.87	5.45	5.28
	PF_g	0.9	0.9	0.9	0.67	0.67	0.67
	P_w (kW)	0.279	0.279	0.279	0.279	0.279	0.279
	Q_d (kVAr)	0.144	0.144	0.142	0.21	0.20	0.19
	v_g (Volt)	420.7	419.4	419.01	603.2	603	599.97

Table 4.7: Performance under synchronization of DFIG with rural grid.

Loading condition	Synchro nization stages	MATLAB Simulation Results (MSR)			Experimental Results (HR)		
		THDVg (%)	THDig (%)	PFg	THDVg (%)	THDig (%)	PFg
Load-1	Weak grid	13.1	7.3	>0.7	14.13	8.45	>0.7
	Transition	14.21	4.14	>0.7	15.27	5.09	>0.7
	Stable	7.51	1.3	0.96	7.88	1.61	0.94
Load-2	Weak grid	14.7	7.9				
	Transition	14.89	4.93				
	Stable	8.3	1.95	0.89			
Load-3	Weak grid	18.74	12.88				
	Transition	22.79	11.89				
	Stable	13.4	5.91	0.83			
Load-4	Weak grid	22.34	17.1				
	Transition	29.02	28.1				
	Stable	15.94	9.23	0.58			

4.6.5 Case-5: Synchronization of DFIG with Rural Grid

The waveforms obtained using the ALMF algorithm for soft synchronization of DFIG into the weak grid (SCR=2.74) at 25% WE penetration are similar to those obtained using the ADALINE-LMS. The WE source and DSTATCOM are connected at 1-second and found that <0.9-s is needed for maintaining soft synchronization. Table 4.7 shows the PQ analysis under the synchronization of DFIG with the rural grid. The observed weak grid, transient (transition) and steady-state (stable) stages voltage and current harmonics are are 14.13%, 15.27%, 7.88% and 8.45%, 5.09%, 1.61%, respectively.

The algorithm's performance has also been tested for different compositions loads by varying the percentage of NL loads (i.e. Load-1=40%, Load-2=50%, Load-3=75% and Load-4=100% NL loads). The harmonics analysis of both simulation and Experimental results are presented in Table 4.7. The results reveal that there is a trade-off between the soft synchronization of DFIG with a high wind penetration level (25%) and the NL loads (beyond 40%). Therefore, such a situation is more challenging and strongly requires more focus.

4.7 HARMONICS AND POWER FLOW ANALYSIS

The harmonics and power analysis of the system without DSTATCOM are illustrated in Fig 4.14 (a). The observed voltage and current harmonic levels are 13.226% and 12.234%, respectively. The active and reactive power are visualized at the PCC are 0.3962 kW/phase and -0.02944 kVAr/phase, respectively. The grid voltage is found to be 203.30 V. These results are not found satisfactory as per the PQ standards.

Figure 4.14 (b) illustrated the harmonics and power analysis with DSTATCOM. The observed voltage and current harmonic levels are 7.69% and 1.95%, respectively and lie within the PQ standards. The active and reactive power are visualized at the PCC are 0.45364 kW/phase and 0.06577 kVAr/phase, respectively. The grid voltage is found to be 239.112 V. These results show that the ALMF controlled DSTATCOM has added the required (0.0363 kVAr/phase) reactive power at the PCC to maintain the grid voltage and harmonic levels at 25% WE penetration level. The grid has been delivered the 0.453kW/phase power (i.e. 1.359 kW) at the PCC. WE source also

delivered the 0.093kW/phase active power (i.e. 0.279 kW) with the rated capacity of 0.400 kW. The total power (1.359 kW + 0.279 kW) supply to the total load of 1.6 kW, depicted in Fig. 4.15 (a), (b). However, negligible power loss (0.04 kW) is observed.

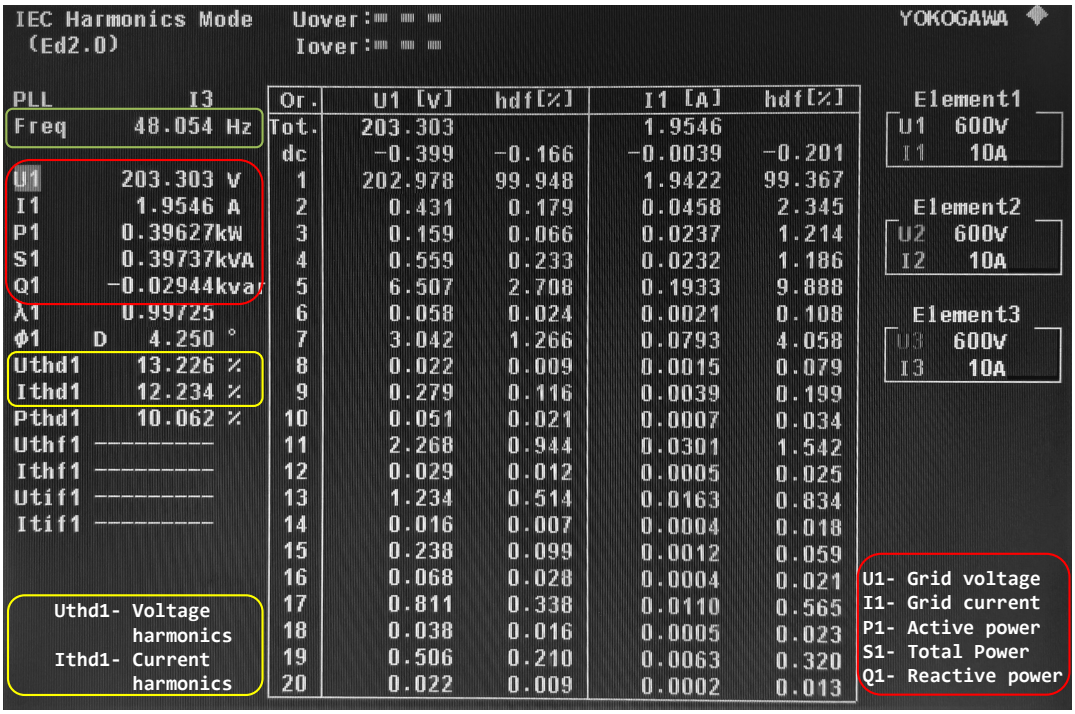

(a)

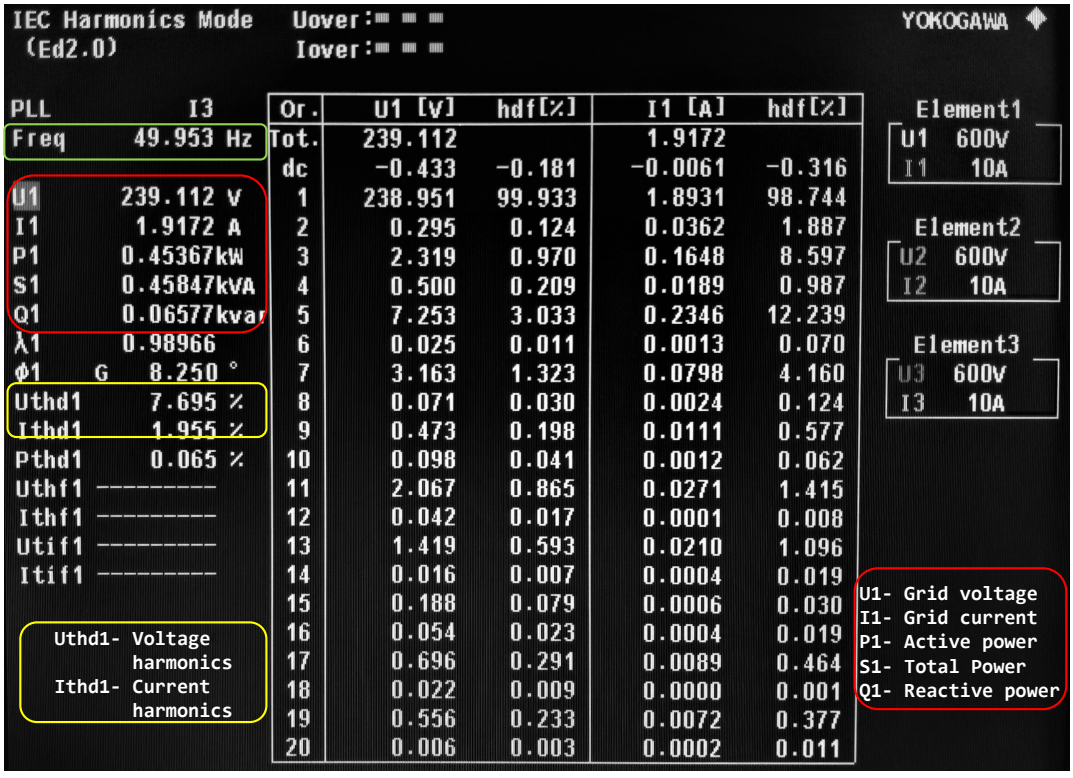

(b)

Figure 4.14: Harmonics and power flow analysis (a) Without DSTATCOM, (b) With DSTATCOM.

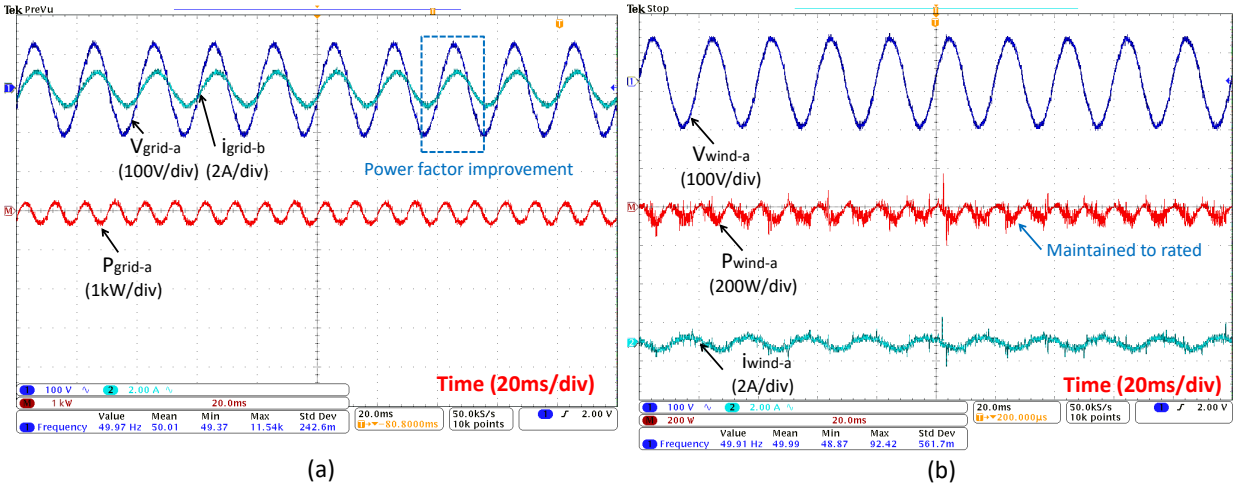

Figure 4.15: Per-phase power analysis (a) Grid, (b) WE source and (c) DSTATCOM.

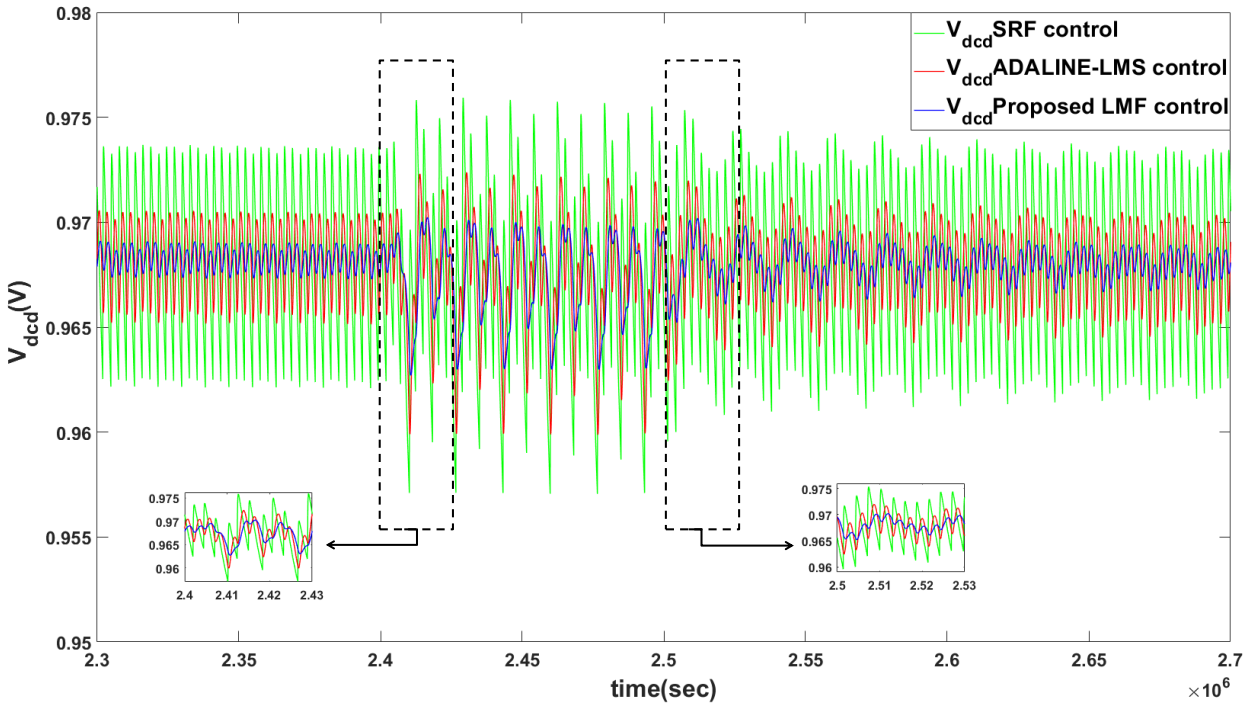

Figure 4.16: DC-link voltage based comparison analysis.

4.8 COMPARATIVE ANALYSIS

The same simulation test has been carried out using Synchronous Reference Frame (SRFT), Adaptive Linear Neural Network-Least Mean Square (ADALINE-LMS) and adaptive LMF control for an SCR of 2.74 with 25% WE penetration. The fluctuations in dc-link voltage of DSTATCOM were found less with the ALMF algorithm compared to the SRF and ADALINE-LMS control algorithm depicted in Fig. 4.16.

Table 4.8 presents the comparison of various algorithms used to enhance WE penetration and the proposed method. The proposed ALMF control is found to be superior in improving power

Table 4.8: Comparative analysis.

Attributes	DSTATCOM with SRFT	DSTATCOM with ADALINE-LMS	DSTATCOM with Proposed ALMF
Computational complexity	High	Low	Low
Accuracy of power estimation	88%	95%	98-100%
Accuracy of voltage tracking	89%	94-96%	96-98%
Voltage harmonics	8.9%	7.89%	7.46%
Current harmonics	3.95%	2.41%	1.52%
Power factor	0.87	0.96	0.99
Stability at SCR < 3	Unstable	Stable	Stable (phase margin -89.8°)
DC-link voltage of DSTATCOM	680 V with high oscillations	680 V with low oscillations	680 V
DC-link voltage of built-in converter	1150 V with high oscillations	1150 V with low oscillations	1150 V
wind power penetration level	$\approx$ 20%	$\approx$ 25%	25%
Reduction in DSTATCOM size	$\approx$ 30-50%	$\approx$ 60-70%	80%

quality and reduction in DSTATCOM size with high WE penetration compared with published algorithms.

4.9 CONCLUSIONS

An Adaptive Least Mean Fourth controlled DSTATCOM method has solved the challenges associated with higher WE penetration levels in the rural grid. The proposed method has been examined for various grid strengths for low SCR with the proliferation of lagging PF inductive and non-linear loads under the variable wind-speed successfully. The outcomes illustrate the capability of proposed research work for rural grid application. The proposed ALMF optimizes DSTATCOM reactive power injection, thereby reducing the size by 80% and providing excellent control over the uncertainties and variability present in the rural grid with 25% WE penetration. The smooth synchronization is also achieved within 0.9 seconds. The simulation and experimental results confirm that the proposed method achieved 25% WE penetration by balancing the load, mitigating harmonics, improving PF and maintaining voltage stability laid by EN-50160 and IEEE 519-2014.